

## Hydrodynamic Anisotropy of Depletion in Nonequilibrium

Lijun Dai,<sup>1</sup> Haixiao Wan,<sup>1</sup> Duo Xu,<sup>1</sup> Xiaobin Dai,<sup>1</sup> Gaojin Li,<sup>2,\*</sup> and Li-Tang Yan<sup>1,†</sup><sup>1</sup>State Key Laboratory of Chemical Engineering, Department of Chemical Engineering, Tsinghua University, Beijing 100084, People's Republic of China<sup>2</sup>School of Naval Architecture, Ocean and Civil Engineering, Shanghai Jiao Tong University, Shanghai 200240, China

(Received 20 December 2022; accepted 1 September 2023; published 27 September 2023)

Active colloids in a bath of inert particles of smaller size cause anisotropic depletion. The active hydrodynamics of this nonequilibrium phenomenon, which is fundamentally different from its equilibrium counterpart and passive particles in an active bath, remains scarcely understood. Here we combine mesoscale hydrodynamic simulation as well as theoretical analysis to examine the physical origin for the active depletion around a self-propelled noninteracting colloid. Our results elucidate that the variable hydrodynamic effect critically governs the microstructure of the depletion zone. Three characteristic states of anisotropic depletion are identified, depending on the strength and stress of activity. This yields a state diagram of depletion in the two-parameter space, captured by developing a theoretical model with the continuum kinetic theory and leading to a mechanistic interpretation of the hydrodynamic anisotropy of depletion. Furthermore, we demonstrate that such depletion in nonequilibrium results in various clusters with ordered organization of squirmers, which follows a distinct principle contrary to that of the entropy scenario of depletion in equilibrium. The findings might be of immediate interest to tune the hydrodynamics-mediated anisotropic interactions and active nonequilibrium organizations in the self-propulsion systems.

DOI: [10.1103/PhysRevLett.131.134002](https://doi.org/10.1103/PhysRevLett.131.134002)

*Introduction.*—The effective interaction arising from the depletion of small particles or depletants around a large colloidal particle is important not only as a fundamental issue of soft matter physics [1–4], but also as that of materials [5–8] and biological science [9–11]: it underlies the behaviors of such disparate systems as flocculation [12], colloidal self-assembly [13–19], and aggregation of red blood cells [20,21]. This interaction in an equilibrium state is usually regarded as entropic force [3,8,22], as was first explained by the established Asakura-Oosawa model [23,24]. However, the entropy scenario is no longer applicable in the systems of active depletion, where the depletants or colloid particle turn into active matters capable of taking up energy from their environment [25–32]. Owing to this continual flow of energy, the active depletion can be understood only in the framework of nonequilibrium physics, which as of now is still in its early stage [33], especially for the case of active colloids immersed in the bath of passive depletants [34–37]. In this case, the perturbed colloid-depletant microstructure generates anisotropic depletion which is fundamentally different from both its equilibrium counterpart [23,24] and passive colloids in the active bath [26–28]. Nevertheless, a fundamental understanding of the physical origin of this anisotropic depletion is far from established, limiting the control and application of such a unique effect in various fields.

Active colloidal particles, such as bacteria and artificial microswimmers, usually self-propel in an embedding fluid, where hydrodynamic interactions (HIs) can be

important [38–42]. These interactions, which essentially originate from momentum and mass conservation of suspensions, are long-ranged and have many-body effects, and sensitively depend on the type of the microswimmer [43–46]. Thus, the hydrodynamics need to be taken into account when rigorously tackling the physical origin of the dynamical depletion regarding active colloids in the fluid bath with passive depletants. However, how active hydrodynamics impacts this nonequilibrium phenomenon has been largely unexplored. The combination of hydrodynamic effects and the inherently stochastic nature of active colloids endows anisotropic depletion with remarkable new interaction patterns and physical principles which are typically not captured by a model without hydrodynamics and remain elusive, leaving an urgent and critical issue to be addressed.

In this Letter, we report on a thorough study of the active hydrodynamic effect on the depletion of passive depletants around a self-propelled noninteracting colloid. We first show by mesoscale hydrodynamic simulations that a variable hydrodynamic effect critically governs the microstructure of depletion zone. Interestingly, depending on the strength and stress of activity, three characteristic states of anisotropic depletion are identified, in striking contrast to that of the counterpart fully or partly neglecting the hydrodynamic effect. This yields a state diagram of depletion in the two-parameter space that provides useful guidance to the control of dynamical depletion. Furthermore, these nonequilibrium features are captured by developing a theoretical model with the continuum kinetic theory, which results in a

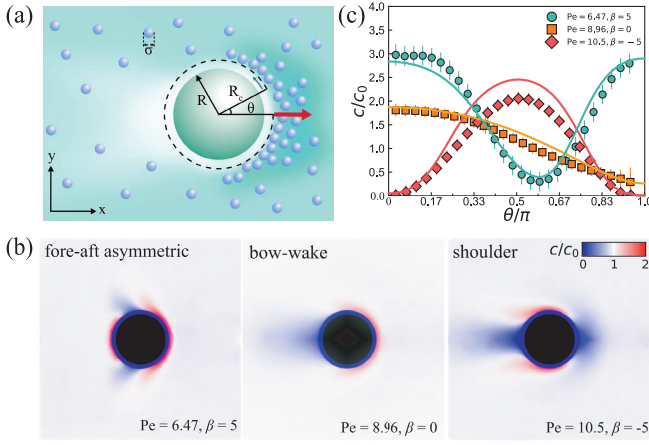


FIG. 1. (a) Sketch of a microswimmer with radius  $R$  self-propelling along the red arrow in a colloidal suspension with size  $\sigma$ . The dashed curve represents the distance  $R_c/R \approx 1.2$ . (b)  $c/c_0$  around the swimmer for  $\beta = 5, 0, -5$  (from left to right). The blue layers indicate colloid-depleted regions, and the red layers indicate colloid-concentrated regions. The swimmer is displayed using the black circle. (c)  $c/c_0$  at  $R_c/R \approx 1.2$  as a function of  $\theta/\pi$ . The solid lines represent the theoretical results. Error bars represent standard deviation.

mechanistic interpretation of the hydrodynamic anisotropy of depletion.

*Simulation.*—We consider a three-dimensional fluid domain containing 5184 small colloidal particles of diameter  $\sigma$  and a squirmer of radius  $R = 3\sigma$ , as sketched in Fig. 1(a), where the squirmer is modeled as a neutral buoyant hard sphere with the prescribed tangential surface velocity [47]. The squirmer is a common model and is widely used to understand flow properties of microorganisms [60–64]. Here, depletion effects in nonequilibrium are discussed through this model. The interaction between the particles is represented by a continuous pseudo-hard-sphere (PHS) potential [65], which has been confirmed to properly describe equilibrium properties [66] as well as out-of-equilibrium features of a hard spherelike fluid [67]. For all systems, the average concentration of colloidal particles is  $c_0 = 0.026$ . To examine collective dynamics of squirmer suspension, we also simulate the system containing multiple squirmers with concentration  $c_{s0} = 0.01$ .  $c_0$  and  $c_{s0}$  are defined as the volumes of the colloidal particle and the squirmer normalized respectively by the volume of the simulation box. Three types of swimmers are considered: a puller ( $\beta < 0$ ), a neutral squirmer ( $\beta = 0$ ), and a pusher ( $\beta > 0$ ), where  $\beta$  represents active stress, characterizing the types of flow field [68]. We employ a hybrid multiparticle collision dynamics (MPCD)-molecular dynamics scheme to simulate the motion of colloidal particles and the squirmer, in which the stochastic-rotation-dynamics variant with angular momentum conservation is applied [69,70]. Full details on the squirmer model, PHS test, and simulation algorithms are presented in the Supplemental Material [47].

In addition, we quantify activity strength via the Péclet number,  $Pe = 2B_1R/3D_0$ , where  $B_1$  is the swimming velocity,  $D_0 \sim k_B T/(3\pi\eta a)$  is the diffusion coefficient of colloidal particles in a passive dilute solution, and  $\eta$  is the solvent viscosity. Physically,  $Pe$  denotes the competition between advection and diffusion effects for the swimmer.

To understand the effects of self-propulsion, we measure azimuthally averaged local colloidal concentration around the squirmer, as shown in Fig. 1(b). In equilibrium, the system stays in a homogeneous state, and a spherical exclusion zone of size  $0.5\sigma$  appears due to the complete depletion of colloidal particles, as illustrated in Fig. S2(a) [47]. However, once the passive swimmer becomes active, the system presents a heterogeneous structure, with the emergence of three characteristic states of anisotropic depletion. Figure 1(c) shows the concentration profile  $c/c_0$  along polar angle  $\theta/\pi$  with respect to the swimming direction at  $R_c/R \approx 1.2$  for these systems, which exhibits remarkable asymmetry. The neutral swimmer moves toward a colloid-rich zone, forming a bow wake and consequently leading to a wakelike zone directly behind the swimmer, consistent with previous results without HIs [26,33]. However, upon  $\beta \neq 0$ , two unexpected new characteristic states emerge, which are distinct from the bow-wake structure. The corresponding concentration distributions develop nonmonotonically in contrast to the monotonic decay of the neutral swimmer. Particularly, at  $\beta = 5$ , a fore-aft asymmetric state is formed, where  $c/c_0$  at the swimmer surface first declines and then increases with increasing  $\theta/\pi$ . The situation is completely opposite at  $\beta = -5$ , where a shoulder depletion zone appears along the swimming axis while colloidal particles reside near the equator of the swimmer.

To assess the detailed range for the emergence of these three anisotropic characteristic states, we systematically explore the variations of microstructures as a function of  $Pe$  and  $\beta$  through examining the angle derivative of particle concentration,  $dc/d\theta$ . Figure S3 shows the angular dependence of  $dc/d\theta$ , where the derivative is always negative at  $\beta = 0$  as  $\theta$  increases, while the gradients are reversed at  $\beta = 5$  and  $\beta = -5$  though they have similar wakelike behaviors. Thus, three characteristic regimes can be discriminated from all self-propelled systems, as marked by the colored circles in Fig. 2(a): the anisotropic microstructure is featured by the fore-aft asymmetric state in the top regime, while in the bottom regime it turns to the shoulder state; within the regime in between, the bow-wake state emerges. The state diagram highlights that these new characteristic states can be regulated by controlling two essential factors regarding active strength  $Pe$  and active stress  $\beta$  [68]. For the sake of providing a detailed insight into the anisotropic states, we analyze the spatial distributions of colloidal particles around a swimmer by calculating polar and nematic order parameters:  $\langle S_1 \rangle$  and  $\langle S_2 \rangle$ . A detailed discussion can be found in the Supplemental Material [47]. Briefly, in a passive system with isotropic

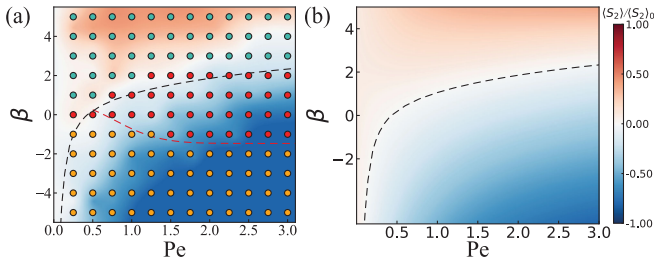


FIG. 2. State diagrams in the  $Pe$ - $\beta$  plane from simulation (a) and theory (b). The symbols denote simulation points with color scheme: fore-aft asymmetric state (olive), bow-wake state (red), and shoulder state (orange). The background color code indicates  $\langle S_2 \rangle / \langle S_2 \rangle_0$ .  $\langle S_2 \rangle_0$  is chosen as 0.12 for simulation and 0.06 for theory. The dashed black line in (a) and (b) is the theoretical prediction for  $\langle S_2 \rangle = 0$ . The red curve in (a) separates the bow-wake and shoulder state by numerically identifying angle derivatives of  $c/c_0$  at  $R_c/R \approx 1.2$  (for more details see the Supplemental Material [47]).

colloidal suspension [Fig. S2(a)],  $\langle S_1 \rangle, \langle S_2 \rangle \rightarrow 0$ . When colloidal particles accumulate to the swimming axis, both these order parameters take the value of 1, while  $\langle S_1 \rangle = 0$  and  $\langle S_2 \rangle = -0.5$  when their positions are located at the swimmer's equator. Thus, combining these two parameters leads to a measure of the alignment degree of colloidal particles with respect to the swimming direction. The results of these parameters well reproduce the above simulations, corroborating that  $Pe$  and  $\beta$  have crucial influence on the heterogeneous distributions of colloidal particles and the formations of anisotropic depletion [47].

Physically,  $\beta$  is related to different far fields of the squirmer [68]. For the weak  $\beta$ , colloidal particles are not sensitive to the far-field behavior. In this case, as the activity strength dominates over the flow fields, the colloidal particles are forced to be transported in the opposite direction of swimming and have not enough time to re-enter the swimmer's end, resulting in a strong front-back asymmetry along the swimming direction, as confirmed by colloidal-particle trajectories [Fig. S6]. For the strong  $\beta$ , the migration pathways and spatial distributions of colloidal particles significantly depend on the types of the far fields. Specifically, in the case of a strong pusher, it generates a thrust from the rear end which pushes neighboring particles away in the swimming direction and does not oppose diffusion of colloidal particles toward the equator, eventually leading to the shoulder state. In view of the fact that  $\beta$  is attributed to the active hydrodynamic effect [68], there seems to be a competitive relationship between  $Pe$  due to the self-propelled speed of the swimmer and HIs arisen from the flow fields, which thereby modifies the anisotropic microstructures of dynamical depletion.

*Theory.*—To further pinpoint the physical origin of the interplay between HIs and  $Pe$  in the characteristic states of anisotropic depletion, we consider a continuum model of colloid suspensions based on the Smoluchowski equation for the conservation of the colloidal particles:

$$\frac{\partial c}{\partial t} + \nabla \cdot (\mathbf{u}_c c) - \frac{1}{Pe} \nabla^2 c = 0, \quad (1)$$

where  $\mathbf{u}_c$  is the colloid velocities [62]. The second term accounts for the convective flux of the colloids, and the last term represents the diffusion of the colloids. Note that velocities are computed in terms of an expression  $v_0 = 2B_1/3$  within the framework of our theoretical model, which can be substituted into  $Pe = v_0 R/D$  and  $D$  is the diffusivity of colloids in a dilute solution. The boundary condition at  $r = 1 + R_c/R$  is expressed as

$$(\mathbf{u}_c \cdot \mathbf{n})c - \frac{1}{Pe} \mathbf{n} \cdot \nabla c = 0, \quad (2)$$

which means that the flux of the colloids vanishes at the surface of the excluded annulus around the squirmer.  $\mathbf{n}$  is the unit normal vector pointing into the fluid.

For colloid suspensions, the velocity  $\mathbf{u}_c = \mathbf{u} + \mathbf{u}_f$  has two contributions, that is, the fluid velocity  $\mathbf{u}$  directly induced by the squirmer

$$\begin{aligned} \mathbf{u} = & \left[ \frac{2}{3} \left( \frac{1}{r^3} - 1 \right) \cos \theta + \frac{\beta}{2} \left( \frac{1}{r^4} - \frac{1}{r^2} \right) (3 \cos^2 \theta - 1) \right] \mathbf{e}_r \\ & + \left[ \frac{2}{3} \left( \frac{1}{2r^3} + 1 \right) \sin \theta + \frac{\beta}{2} \frac{1}{r^4} \sin 2\theta \right] \mathbf{e}_\theta, \end{aligned} \quad (3)$$

and the velocity correction  $\mathbf{u}_f$  due to the repulsive potential between the squirmer and colloid as well as finite size of the colloid. For simplicity, we only account for the far-field HI represented by Faxen's law [71]:

$$\mathbf{u}_f = \frac{R_c^2}{6R^2} \nabla^2 \mathbf{u}. \quad (4)$$

We numerically solve Eq. (1) using the finite difference method [72]. Figure 3(a) gives the representative theoretical profiles, in qualitative agreement with the simulated microstructures in Fig. 1(b). Given the same parameters, this model can quantitatively reproduce the dependence of concentration distribution on  $\theta$  from the simulations, despite the existence of the local bias due to the approximation of the continuum model and perhaps the fluctuations of numerical data. Moreover, Fig. 2(b) shows the theoretical variations of anisotropic microstructures in terms of the parameter  $\langle S_2 \rangle$ . In comparison to Fig. 2(a), a qualitative agreement between the simulated and theoretical results can be identified, indicating the universal nature of anisotropic depletionlike microstructures in these self-propelled systems. In particular, the plot with  $\langle S_2 \rangle = 0$  inferred from the contour lines of the state diagram of the theoretical model provides a reasonable boundary criterion for distinguishing the fore-aft asymmetric state from the other two types of states. Besides, one can observe that the local concentration of colloidal particles on the surface of the neutral swimmer is smaller than those of the other two cases since the flow field is not long ranged and decays as  $\sim r^{-3}$ ; recall that in a Newtonian liquid, the magnitude of

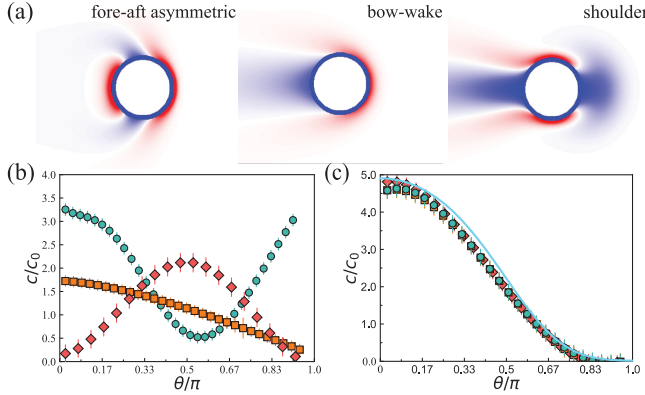


FIG. 3. (a) Representative distribution of local colloidal particle concentration around the swimmer using the continuum theory for  $\beta = 5, 0, -5$  (from left to right).  $c/c_0$  at  $R_c/R \approx 1.2$  as a function of  $\theta/\pi$ , with fixed squirmer (b) and without HIs (c) for  $\beta = 5, 0, -5$ . Same symbols, Pe, and color code as in Fig. 1. The solid line in (c) represents the theoretical dependence on  $\theta$  given by Eq. (5). Error bars represent the standard deviation.

velocity field for  $\beta \neq 0$  obeys the formula  $\sim r^{-2}$  due to force dipole [73]. Overall, although the near-field interactions and the details of particle-to-particle interactions are ignored, this hydrodynamic model reasonably captures the simulated results, underscoring the critical role of HIs in the anisotropic states of active depletion.

*Discussion.*—While this continuum model has stressed the role of HIs in anisotropic characteristic states, it appears from the above results that Pe related to the self-propulsion speed also affects these microstructures. Consequently, we provide a more definite evaluation of the separate contribution of both of these factors through switching off one of them.

First, the squirmer is fixed by an external force so that the effect of squirmer motion can be determined. Figure 3(b) shows  $c/c_0$  near the swimmer as a function of  $\theta/\pi$ , with their shapes similar to those of the system with a free squirmer [Fig. S7(a)]. In combination with Fig. 2(a) as well as the detailed analysis of additional calculations [Figs. S8–S9], one can find that squirmer motion has a relatively light effect on the structure of anisotropic depletions, but can evidently modify their amplitudes. Effectively, it can considerably affect the flow field [Figs. S7(b)–S7(d)], and thereby contribute to extra HIs.

Next, additional simulations without HI effects are performed, in which the MPCD collision step is replaced by the random velocity and position resampling of the fluid particles, commonly referred to as a repositioning (RP) scheme [74]. Figure S2(b) shows the mean square displacement of colloidal particles considered through the MPCD and RP scheme, respectively. A faster movement is observed for the MPCD system, suggesting that HI effects can accelerate the dynamics of particles [75]. Furthermore, we measure  $c/c_0$  at  $R_c/R \approx 1.2$  [Fig. 3(c)]. In sharp contrast to the results from MPCD, the concentration

profiles of these three types of swimmers exhibit the same behavior of monotonic decay, all of which show high-density regions in front of the swimmer and long-ranged low-density regions in the wake region behind the self-propelled particle [Fig. S9], as observed in other similar nonequilibrium systems without HIs [26,33].

Last, we consider these self-propelled systems without HI effects based on our theoretical model. This is implemented by using the constant translational velocity  $\mathbf{u}_c = 2B_1/3(-\cos\theta\mathbf{e}_r + \sin\theta\mathbf{e}_\theta)$ , which is considered as the head-on collision between colloidal particles and the squirmer. In the low Pe limits, the perturbation theory predicts that  $c \sim 1 + \text{Pe} \cos\theta/2$  [72]. For  $\text{Pe} \gg 1$ , the boundary layer theory shows that the same result is derived for the leading side of the sphere ( $\theta < \pi/2$ ). For the full region, we find that the colloidal concentration at the sphere surface can be approximated by

$$c \sim \text{Pe}(1 + \cos\theta)/4, \quad (5)$$

which is directly dependent on Pe. Figure 3(c) shows that the theoretical prediction on the excluded annulus through Eq. (5) well captures the simulations.

The above results allow us to conclude that the anisotropy of active depletion emerging in these nonequilibrium systems is, in nature, determined by HIs. It may have broad implications for the interactions and nonequilibrium organizations of diverse microorganisms and artificial active matters. In essence, the hydrodynamics-mediated *anisotropic* depletion causes the broken symmetry of the interactions, which endows the microswimmers with virtual properties of long-ranged specificity and directionality, and consequently regulates dynamical organizations and collective behaviors. To demonstrate this point, we extend the simulations to collective dynamics of the squirmer suspension with passive depletants of noninteractive colloids. Figure 4 shows the spatial distribution and dynamical structures of the squirmers. Indeed, hydrodynamic anisotropy of depletion in nonequilibrium can drive the squirmers to form various clusters with ordered organization

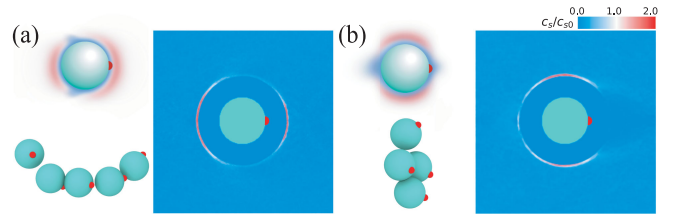


FIG. 4. Upper left corner: sketches of colloidal particle distribution around the swimmer. Lower left corner: typical collective states formed by squirmers, which form ordered clusters of active chain (a) and swarm (b), respectively. Right: spatial distribution of the squirmers around a central squirmer, where the color code on the top right indicates squirmer concentration  $c_s/c_{s0}$ , for  $\beta = 5$  (a) and  $\beta = -5$  (b) at  $\text{Pe} = 3.0$ . Green sphere: the squirmer whose swimming direction is indicated by red dots.

related to the propulsion mechanism. More importantly, the assembly sites for squirmers occur in the aggregation zone of colloidal particles instead of the depletion zone, revealing that structural organization governed by such depletion in nonequilibrium follows a distinct principle contrary to that of the entropy scenario of depletion in equilibrium [76], where HIs overwhelm entropic force and thereby dominate this behavior. This offers new approaches to tune such dynamical interactions and organization in nonequilibrium. Furthermore, it also suggests a unique way of understanding various behaviors of the microorganisms, including their intercolony communication, nutrient uptake, and swarming mobility [77–79]. For example, the correlation between propulsion mechanism and the characteristics of flow field in the surrounding environment may play a critical role in the locomotion strategies of diverse microorganisms [77,80,81].

*Conclusions.*—We found three characteristic states of anisotropic depletion in nonequilibrium through considering the hard spherelike squirmer as a self-propelled swimmer. By constructing a state diagram, we demonstrated that these states can be quantitatively regulated by two essential factors:  $Pe$  due to the self-propelled speed of the swimmer and  $\beta$  related to the flow fields. We further developed a hydrodynamic continuum model, capturing the simulations and verifying the universality of the anisotropic depletion microstructures in these systems. Our results have revealed that hydrodynamic interactions induced by the swimmers fundamentally determine anisotropic depletion states. Furthermore, we demonstrate that such depletion in nonequilibrium results in various clusters with ordered organization of squirmers, which follows a distinct principle contrary to that of the entropy scenario of depletion in equilibrium. The findings could provide the cornerstone for understanding and controlling hydrodynamics-mediated anisotropic interactions and nonequilibrium organizations in the self-propulsion systems, artificial or biological.

We thank Kai Qi, Xiaqing Shi, Ran Ni, Mingcheng Yang, Zhaoyan Sun, Zhenyue Yang, and Youliang Zhu for stimulating discussions. We acknowledge support from the National Natural Science Foundation of China (Grant No. 22025302, No. 21873053, No. 12102258, and No. 12372264). L. T. Y. acknowledges financial support from Ministry of Science and Technology of China (Grant No. 2022YFA1200061) and State Key Laboratory of Chemical Engineering (No. SKL-ChE-23T01).

\*Corresponding author: gaojinli@sju.edu.cn

†Corresponding author: ltyan@mail.tsinghua.edu.cn

- [1] H. N. W. Lekkerkerker and R. Tuinier, *Colloids and the Depletion Interaction* (Springer, New York, 2011).  
 [2] P. J. Lu, E. Zaccarelli, F. Ciulla, A. B. Schofield, F. Sciortino, and D. A. Weitz, *Nature (London)* **453**, 499 (2008).

- [3] G. van Anders, D. Klotsa, N. K. Ahmed, M. Engel, and S. C. Glotzer, *Proc. Natl. Acad. Sci. U.S.A.* **111**, E4812 (2014).  
 [4] J. Ruiz-Franco and E. Zaccarelli, *Annu. Rev. Condens. Matter Phys.* **12**, 51 (2021).  
 [5] M. J. Bergman, N. Gnan, M. Obiols-Rabasa, J.-M. Meijer, L. Rovigatti, E. Zaccarelli, and P. Schurtenberger, *Nat. Commun.* **9**, 1 (2018).  
 [6] W. Knoben, N. A. M. Besseling, and M. A. Cohen Stuart, *Phys. Rev. Lett.* **97**, 068301 (2006).  
 [7] Y. Wang, Y. Wang, D. R. Breed, V. N. Manoharan, L. Feng, A. D. Hollingsworth, M. Weck, and D. J. Pine, *Nature (London)* **491**, 51 (2012).  
 [8] G. Zhu, Z. Huang, Z. Xu, and L.-T. Yan, *Acc. Chem. Res.* **51**, 900 (2018).  
 [9] A. Stradner, H. Sedgwick, F. Cardinaux, W. C. Poon, S. U. Egelhaaf, and P. Schurtenberger, *Nature (London)* **432**, 492 (2004).  
 [10] F. Cardinaux, T. Gibaud, A. Stradner, and P. Schurtenberger, *Phys. Rev. Lett.* **99**, 118301 (2007).  
 [11] H. Kang, N. M. Toan, C. Hyeon, and D. Thirumalai, *J. Am. Chem. Soc.* **137**, 10970 (2015).  
 [12] P. Jenkins and M. Snowden, *Adv. Colloid Interface Sci.* **68**, 57 (1996).  
 [13] D. J. Kraft, R. Ni, F. Smallenburg, M. Hermes, K. Yoon, D. A. Weitz, A. van Blaaderen, J. Groenewold, M. Dijkstra, and W. K. Kegel, *Proc. Natl. Acad. Sci. U.S.A.* **109**, 10787 (2012).  
 [14] T. Schilling, S. Jungblut, and M. A. Miller, *Phys. Rev. Lett.* **98**, 108303 (2007).  
 [15] C. Mayer, E. Zaccarelli, E. Stiakakis, C. Likos, F. Sciortino, A. Munam, M. Gauthier, N. Hadjichristidis, H. Iatrou, P. Tartaglia *et al.*, *Nat. Mater.* **7**, 780 (2008).  
 [16] V. J. Anderson and H. N. Lekkerkerker, *Nature (London)* **416**, 811 (2002).  
 [17] F. Zosel, A. Soranno, K. J. Buholzer, D. Nettel, and B. Schuler, *Proc. Natl. Acad. Sci. U.S.A.* **117**, 13480 (2020).  
 [18] G. Meng, N. Arkus, M. P. Brenner, and V. N. Manoharan, *Science* **327**, 560 (2010).  
 [19] S. Sacanna, W. T. Irvine, P. M. Chaikin, and D. J. Pine, *Nature (London)* **464**, 575 (2010).  
 [20] B. Neu and H. J. Meiselman, *Biophys. J.* **83**, 2482 (2002).  
 [21] G. Zhu, Z. Xu, and L.-T. Yan, *Nano Lett.* **20**, 5616 (2020).  
 [22] V. N. Manoharan, *Science* **349**, 1253751 (2015).  
 [23] S. Asakura and F. Oosawa, *J. Chem. Phys.* **22**, 1255 (1954).  
 [24] S. Asakura and F. Oosawa, *J. Polym. Res.* **33**, 183 (1958).  
 [25] C. Bechinger, R. Di Leonardo, H. Löwen, C. Reichhardt, G. Volpe, and G. Volpe, *Rev. Mod. Phys.* **88**, 045006 (2016).  
 [26] J. Dzubiella, H. Löwen, and C. N. Likos, *Phys. Rev. Lett.* **91**, 248301 (2003).  
 [27] L. Angelani, C. Maggi, M. L. Bernardini, A. Rizzo, and R. Di Leonardo, *Phys. Rev. Lett.* **107**, 138302 (2011).  
 [28] T. Speck and A. Jayaram, *Phys. Rev. Lett.* **126**, 138002 (2021).  
 [29] S. Paul, A. Jayaram, N. Narinder, T. Speck, and C. Bechinger, *Phys. Rev. Lett.* **129**, 058001 (2022).  
 [30] R. Ni, M. A. Cohen Stuart, and P. G. Bolhuis, *Phys. Rev. Lett.* **114**, 018302 (2015).  
 [31] P. Liu, S. Ye, F. Ye, K. Chen, and M. Yang, *Phys. Rev. Lett.* **124**, 158001 (2020).

- [32] J. Zhang, R. Alert, J. Yan, N. S. Wingreen, and S. Granick, *Nat. Phys.* **17**, 961 (2021).
- [33] R. Wulfert, U. Seifert, and T. Speck, *Soft Matter* **13**, 9093 (2017).
- [34] J. Katuri, W. E. Usual, M. N. Popescu, and S. Sánchez, *Sci. Adv.* **7**, eabd0719 (2021).
- [35] K. Singh, A. Yadav, P. Dwivedi, and R. Mangal, *Langmuir* **38**, 2686 (2022).
- [36] A. S. Khair and J. F. Brady, *Proc. R. Soc. A* **463**, 223 (2007).
- [37] M. Krüger and M. Rauscher, *J. Chem. Phys.* **127**, 034905 (2007).
- [38] M. C. Marchetti, J.-F. Joanny, S. Ramaswamy, T. B. Liverpool, J. Prost, M. Rao, and R. A. Simha, *Rev. Mod. Phys.* **85**, 1143 (2013).
- [39] A. Zöttl and J. M. Yeomans, *Nat. Phys.* **15**, 554 (2019).
- [40] Y. Sokolov, D. Frydel, D. G. Grier, H. Diamant, and Y. Roichman, *Phys. Rev. Lett.* **107**, 158302 (2011).
- [41] K. Schaar, A. Zöttl, and H. Stark, *Phys. Rev. Lett.* **115**, 038101 (2015).
- [42] G. Li and A. M. Ardekani, *Phys. Rev. Lett.* **117**, 118001 (2016).
- [43] K. Qi, E. Westphal, G. Gompper, and R. G. Winkler, *Phys. Rev. Lett.* **124**, 068001 (2020).
- [44] J. L. Aragoes, S. Yazdi, and A. Alexander-Katz, *Phys. Rev. Fluids* **3**, 083301 (2018).
- [45] J. Stenhammar, R. Wittkowski, D. Marenduzzo, and M. E. Cates, *Phys. Rev. Lett.* **114**, 018301 (2015).
- [46] R. Niu, T. Palberg, T. Speck *et al.*, *Phys. Rev. Lett.* **119**, 028001 (2017).
- [47] See Supplemental Material at <http://link.aps.org/supplemental/10.1103/PhysRevLett.131.134002> for additional information about the details of the squirmer model and simulation methods, interparticle interaction, passive suspension, and self-propulsion systems, which includes Refs. [48–59].
- [48] C. C. Huang, G. Gompper, and R. G. Winkler, *Phys. Rev. E* **86**, 056711 (2012).
- [49] K. Qi, E. Westphal, G. Gompper, and R. G. Winkler, *Commun. Phys.* **5**, 49 (2022).
- [50] T. Ihle and D. M. Kroll, *Phys. Rev. E* **63**, 020201(R) (2001).
- [51] C. C. Huang, A. Chatterji, G. Sutmann, G. Gompper, and R. G. Winkler, *J. Comput. Phys.* **229**, 168 (2010).
- [52] E. Westphal, S. P. Singh, C. C. Huang, G. Gompper, and R. G. Winkler, *Comput. Phys. Commun.* **185**, 495 (2014).
- [53] M. Hecht, J. Harting, T. Ihle, and H. J. Herrmann, *Phys. Rev. E* **72**, 011408 (2005).
- [54] M. Theers, Mesoscale hydrodynamic simulations: From a single colloid to the collective dynamics of microswimmers, Ph.D. thesis, RWTH Aachen University, 2017.
- [55] M. Ripoll, K. Mussawisade, R. G. Winkler, and G. Gompper, *Phys. Rev. E* **72**, 016701 (2005).
- [56] M. T. Downton and H. Stark, *J. Phys. Condens. Matter* **21**, 204101 (2009).
- [57] N. F. Carnahan and K. E. Starling, *J. Chem. Phys.* **51**, 635 (1969).
- [58] D. Saintillan and M. J. Shelley, *Phys. Rev. Lett.* **99**, 058102 (2007).
- [59] X. Chen, X. Dong, A. Be'er, H. L. Swinney, and H. P. Zhang, *Phys. Rev. Lett.* **108**, 148101 (2012).
- [60] M. J. Lighthill, *Commun. Pure Appl. Math.* **5**, 109 (1952).
- [61] J. R. Blake, *J. Fluid Mech.* **46**, 199 (1971).
- [62] D. Saintillan and M. J. Shelley, *Phys. Rev. Lett.* **100**, 178103 (2008).
- [63] T. Ishikawa, J. Locsei, and T. J. Pedley, *J. Fluid Mech.* **615**, 401 (2008).
- [64] T. Ishikawa, M. P. Simmonds, and T. J. Pedley, *J. Fluid Mech.* **568**, 119 (2006).
- [65] J. Jover, A. Haslam, A. Galindo, G. Jackson, and E. Müller, *J. Chem. Phys.* **137**, 144505 (2012).
- [66] F. Pousaneh and A. S. de Wijn, *Phys. Rev. Lett.* **124**, 218004 (2020).
- [67] W. Gispén and M. Dijkstra, *Phys. Rev. Lett.* **129**, 098002 (2022).
- [68] A. Zöttl and H. Stark, *Phys. Rev. Lett.* **112**, 118101 (2014).
- [69] G. Gompper, T. Ihle, D. Kroll, and R. Winkler, *Adv. Polym. Sci.* **221**, 1 (2009).
- [70] M. Theers, E. Westphal, G. Gompper, and R. G. Winkler, *Phys. Rev. E* **93**, 032604 (2016).
- [71] S. Kim and S. J. Karrila, *Microhydrodynamics: Principles and Selected Applications* (Courier Corporation, Boston, 2013).
- [72] T. M. Squires and J. F. Brady, *Phys. Fluids* **17**, 073101 (2005).
- [73] A. Zöttl and H. Stark, *J. Phys. Condens. Matter* **28**, 253001 (2016).
- [74] M. Belushkin, R. Winkler, and G. Foffi, *Soft Matter* **8**, 9886 (2012).
- [75] A. Chen, N. Zhao, and Z. Hou, *Soft Matter* **13**, 8625 (2017).
- [76] M. Liu, X. Zheng, V. Grebe, D. J. Pine, and M. Weck, *Nat. Mater.* **19**, 1354 (2020).
- [77] M. B. Short, C. A. Solari, S. Ganguly, T. R. Powers, J. O. Kessler, and R. E. Goldstein, *Proc. Natl. Acad. Sci. U.S.A.* **103**, 8315 (2006).
- [78] Y. Peng, Z. Liu, and X. Cheng, *Sci. Adv.* **7**, eabd1240 (2021).
- [79] S. Liu, S. Shankar, M. C. Marchetti, and Y. Wu, *Nature (London)* **590**, 80 (2021).
- [80] H. C. Berg and L. Turner, *Nature (London)* **278**, 349 (1979).
- [81] S. Till, F. Ebmeier, A. A. Fragkopoulos, M. G. Mazza, and O. Bäumchen, *Phys. Rev. Res.* **4**, L042046 (2022).